Chemical Physics Letters 700 (2018) 36–43

Contents lists available at ScienceDirect

Chemical Physics Letters

journal homepage: www.elsevier.com/locate/cplett

Research paper

Energy-switching potential energy surface for ground-state C_3

C.M.R. Rocha, A.J.C. Varandas *

Department of Chemistry and Coimbra Chemistry Center, University of Coimbra, 3004-535 Coimbra, Portugal

ARTICLE INFO

Article history:
Received 1 February 2018
In final form 3 April 2018
Available online 5 April 2018

Keywords:
C_3
Potential energy surfaces
Energy switching
Rovibrational spectroscopy

ABSTRACT

The multiple energy switching scheme [J. Chem. Phys. 119 (2003) 2596] has been used to improve the double many-body expansion (DMBE II) potential energy surface of C_3 near its linear global minima by morphing it with an accurate Taylor-series expansion [J. Chem. Phys. 144 (2016) 044307]. The final ES form attains the accuracy of the local form in reproducing the rovibrational spectrum of C_3 while keeping unaltered all key attributes of the original DMBE II, namely conical intersection seams and dissociative channels. The ES form is therefore commended for adiabatic spectroscopic and reaction dynamics studies.

1. Introduction

In principle, a global potential energy surface (PES) is expected to reproduce experimental data at regions of the nuclear configuration space where such information is available, and behave in a physically reasonable manner elsewhere (namely, at intermediate and long-range regions) [1–4]. In practice, such a requirement is seldom fulfilled. Despite all recent computational/methodological developments, the above problem still poses a challenge to both *ab initio* theory and analytical modeling [5], particularly if aiming at spectroscopic accuracy [6–21] (the list is by no means complete, with references to other work being obtainable by cross-referencing).

This led one of us [6] to suggest a simple, yet reliable, scheme in which two potential forms [$V_1(\mathbf{R})$ and $V_2(\mathbf{R})$] optimal at distinct energy regimes can be merged together and switched smoothly from one to the other as a function of energy such that the final energy switching (ES) form is accurate everywhere [6,7,9,14]. As usual, $V_1(\mathbf{R})$ is a double many-body expansion (DMBE)-type [4,22] function or any global form that warrants a realistic description of the whole surface including the location and well depth of the potential minimum(a). In turn, $V_2(\mathbf{R})$ is a local-type form that attains spectroscopic accuracy near such minimum(a). The ES potential ($V_{\rm ES}$) is then given by [6]

$$V_{\rm ES} = f(\Delta E)V_1(\mathbf{R}) + [1 - f(\Delta E)]V_2(\mathbf{R}), \tag{1}$$

with

$$f(\Delta E) = \frac{1}{2}\{1 + \tanh[(\gamma_0 + \gamma_1 \Delta E^m)\Delta E]\}, \tag{2}$$

where $\Delta E = E - E_0$ is the displacement from some reference energy E_0 at which $V_1(\mathbf{R})$ and $V_2(\mathbf{R})$ are equally reliable, and $f(\Delta E)$ is a switching function that ensures $V_{\rm ES} \equiv V_2(\mathbf{R})$ for large negative energy displacements (at the absolute minimum) and $V_{\rm ES} \equiv V_1(\mathbf{R})$ for large positive ones (at the atom-diatom dissociation limits). In turn, γ_i $(i = 0, 1)$ are disposable parameters to be optimized for a selected even power of m [6]. Clearly, $V_{\rm ES}$ benefits from the advantages of both individual forms, while avoiding their limitations [6,7,9]. The ES scheme has proved effective in obtaining spectroscopically accurate global PESs for H_2O [6,7,9,17], H_3^+ [8,11] and also for systems such as ArHCN [23], HO_3 [24] and HeHCN [25].

Recently, Varandas suggested further refinements onto the approach by introducing the multiple ES (MES) scheme [14]. The novel methodology is particularly useful to convey spectroscopic accuracy for systems in which the switching from $V_2(\mathbf{R})$ to $V_1(\mathbf{R})$ takes place in a narrow energy window, as is the case for $NO_2(1^2A')$ [14]. Accordingly, the ES potential ($V'_{\rm ES}$) assumes the form [14]

$$V'_{\rm ES} = f'_i \ldots f'_3 f'_2 f'_1 [V_1(\mathbf{R}) - V_2(\mathbf{R})] + V_2(\mathbf{R}), \tag{3}$$

with the switching functions f'_i being defined by [14]

$$f'_i(\Delta E') = \begin{cases} \exp\left[-\beta_i \left(\frac{\Delta E'_0}{\Delta E' + \xi} - 1\right)^{n_i}\right] & \text{if } \Delta E' < \Delta E'_0 \\ 1 & \text{if } \Delta E' \geqslant \Delta E'_0. \end{cases} \tag{4}$$

In the above equation, $\Delta E' = E - E_{\rm min}$ is the energy displacement with respect to the absolute minimum of the global PES, while $\Delta E'_0 = E'_0 - E_{\rm min}$ measures the energy difference between $E_{\rm min}$ and

* Corresponding author.
E-mail address: varandas@uc.pt (A.J.C. Varandas).

https://doi.org/10.1016/j.cplett.2018.04.005
0009-2614/

some cutoff energy E_0' [14]. Typically, E_0' can be judiciously chosen in such a way as to keep unaltered some chosen topographical feature of $V_1(\mathbf{R})$ (*e.g.*, a conical intersection [14]) or simply represent the energy threshold at which the Taylor-series-expansion-type form $V_2(\mathbf{R})$ is valid. In turn, β_i is a trial-and-error parameter, n_i is an even integer and ξ is a small number chosen to avoid numerical overflows at $E = E_{\min}$.

The present work is concerned with $C_3(1^1A')$, an astrophysically relevant species that plays a central role in the chemistry of cometary and interstellar atmospheres [26,27]. Recently, the authors reported [28] an *ab initio*-based global PES (DMBE I) for the ground electronic state of the title species. A total of 629 *ab initio* energies calculated at the multireference configuration interaction (MRCI) level of theory and the aug-cc-pV*T*Z (AV*T*Z) [29] basis have been employed. The input *ab initio* data have been there also scaled to account for the incompleteness of the one- and $\mathcal{N}$-electron basis via DMBE-scaled external correlation (DMBE-SEC) method [30] and subsequently fitted with a root mean square deviation (rmsd) of 346 cm^{-1} [28]. To judge the quality of the potential form so obtained, exploratory rovibrational energy calculations have been performed. As shown in the original paper [28], the DMBE I PES reproduces the vibrational energy spectrum of C_3 with a rmsd of 50.4 cm^{-1} for 53 calculated levels up to about 3000 cm^{-1} above zero point energy (ZPE) [28]. Most recently, the authors reported [31] a refined form (DMBE II) which has been especially designed to properly mimic the region defined by the 4 conical intersections in the title molecule, which are due to combined Jahn-Teller plus pseudo-Jahn-Teller $[(E' + A_1') \otimes e']$ vibronic effects [28,31,32]. For this, the *ab initio* data set was extended to a total of 1050 grid points and least-squares fitted to the DMBE II form with a rmsd of 340 cm^{-1}.

As stated elsewhere [28], the above global PESs could provide the required input for further improvements to true spectroscopic accuracy via the ES scheme [6,14]. Of course, the first step toward such an approach consists of selecting available local forms that fulfill the desired requirements. As emphasized by van Orden and Saykally [26], the carbon trimer is one of the most well-characterized nonrigid triatomics in existence and such a wealth of experimental and theoretical effort has been devoted in obtaining accurate near-equilibrium ground-state PESs for the title species [10,15,33–35].

Of special relevance is the purely *ab initio* local form of Schröder and Sebald (SS) [35]. These authors report a near-equilibrium PES for ground-state C_3 from a composite approach based on accurate fc-CCSD(T*)-F12b/AV5Z ("fc" stands for frozen core) energies [35] corrected additively to approximate higher-order correlations (up to iterative pentuples CCSDTQP), core-core/core-valence effects, and scalar relativistic contributions. All calculated energies were then fitted to a polynomial form with a standard deviation of only 0.05 cm^{-1} [35]. It should be pointed out that their work is primarily concerned with low-lying rotation-vibration energies obtained for $J \leq 30$ (where J denotes the total angular momentum quantum number) but a few vibrational energies up to ≈ 3500 cm^{-1} above ZPE were also reported. As shown by the authors [35], their local form mimics such data within 1 cm^{-1}.

In the present work, the SS local form [35] is merged with DMBE II [31] by following Varandas' [14] MES scheme [Eqs. (3) and (4)]. Inspired by the graphical abstract, the resulting ES potential will be called DMBE II/ES/SS, although we remove "II" for simplicity. To judge its quality, rovibrational calculations are performed and the results compared with the SS ones. Although primarily concerned with the SS form, we also assess the accuracy of previous Taylor series expansions due to Ahmed et al. (ABW) [15], Mladenović et al. (MSB) [34] and Špirko et al. (SMJ) [10] in reproducing the rovibrational spectrum of C_3.

The plan of the paper is as follows. In Section 2, we provide some aspects of the current ES methodology employed for ground-state C_3 and also show the main topographical features of the resulting ES potential. The details of the rovibrational energy calculations here performed are described in Section 3, while the results and discussion are in Section 4. Section 5 gathers the conclusions.

2. The ES potential energy surface

Since the SS [35] and DMBE II [31] potentials are exceptionally flat near the region defined by the linear global minimum (Min) [see Fig. 1], only a single switching function $f_1'(\Delta E') \equiv f'(\Delta E')$ with $n_1 \equiv n = 2$ [see Eqs. (3) and (4)] suffices to smoothly connect the above PESs (for brevity, the corresponding functional forms will not be given here, with the reader being addressed to the original papers for details). As usual, $\beta_1 \equiv \beta$ has been determined from the requirement that $V_{\rm ES}'$ approaches the accuracy of the original local PES in reproducing the rovibrational data (see later), while avoiding the appearance of wrinkles close to the reference E_0' [14]. To assess the role of β on the final ES form, we have considered two DMBE/ES/SS variants: one with a mild transition ($\beta = 10$) and another with $\beta = 50$. The parameters used are summarized in Table 1.

The topographical features of the final ES global potential are depicted in Figs. 1 and 2. Also shown is the corresponding SS local PES. Moreover, Fig. S1 of the Supplementary Material (SM) and 2 illustrate the near-equilibrium ABW [15], MSB [34] and SMJ [10] PESs; see Tables 2 and 3 for the structural parameters of the Min geometries and ZPEs predicted from all potential forms [10,15,34,35]. Note that we ensured invariance of all local potentials with respect to permutation of the C atoms.

Some remarks are due on the determination of the cutoff energy E_0' in Eq. (4). First, the original crossing seams of D_{3h} and C_{2v} symmetries [28,31,32] (which occur at $E_{\rm Ci} = 0.0515$ E_h (11302 cm^{-1}) above the Min structure) must be kept as in DMBE II. Second, the SS local form cannot describe the isomerization transition state TS_{iso} at $E_{TS} = 0.0341$ E_h (7482 cm^{-1}) as is the case for any Taylor series expansion; see Fig. 1(b) and S1. Thus, the switching from SS to DMBE II must occur before this regime. Recall also that the local SS form depicts several spurious holes at regions close to equilateral triangular conformations (these unphysical features are delimited by the magenta triangle in Fig. 1). Since Schröder and Sebald [35] utilized in their fit geometries up to $\phi = 80°$, we judged convenient to define E_0' at 0.0285 E_h (6250 cm^{-1}) above Min. This is indicated by the navy dashed contours in Fig. 1(a) and the black dotted line in the one-dimensional cuts of Fig. 2. Note that $E_{\min}$ in Eq. (4) is set to the energy of the $D_{\infty h}$ global minimum (Table 1), with E determined from the global DMBE II form.

Regarding ABW [15], their Taylor-series expansion was calibrated from 384 MRCI(Q)/V*T*Z energies with a few of the potential parameters subsequently refined to mimic experimental data. Covering a range of ≈ 8713 cm^{-1} above ZPE and reproducing 100 observed rovibrational levels to within 3 cm^{-1}, such a fit [15] treated the lowest eigenvalue $(0,0^0,0)$ as an *ad hoc* parameter, with the claimed accuracy being reproduced only when the ZPE is fixed at their recommended value of 1728.1 cm^{-1}; see later. Thence, there is no reported potential form that reproduces their scaled rovibrational spectra. In fact, the true calculated ZPE level from their potential is 1720.5 cm^{-1}; see Table 3. Stated differently, their local form cannot be employed without risk in the morphing procedure with DMBE II: when doing so, the resulting ES PES shows visible scars (due to the distinct geometrical parameters) while persisting the difficulty of defining a proper ZPE for reference.

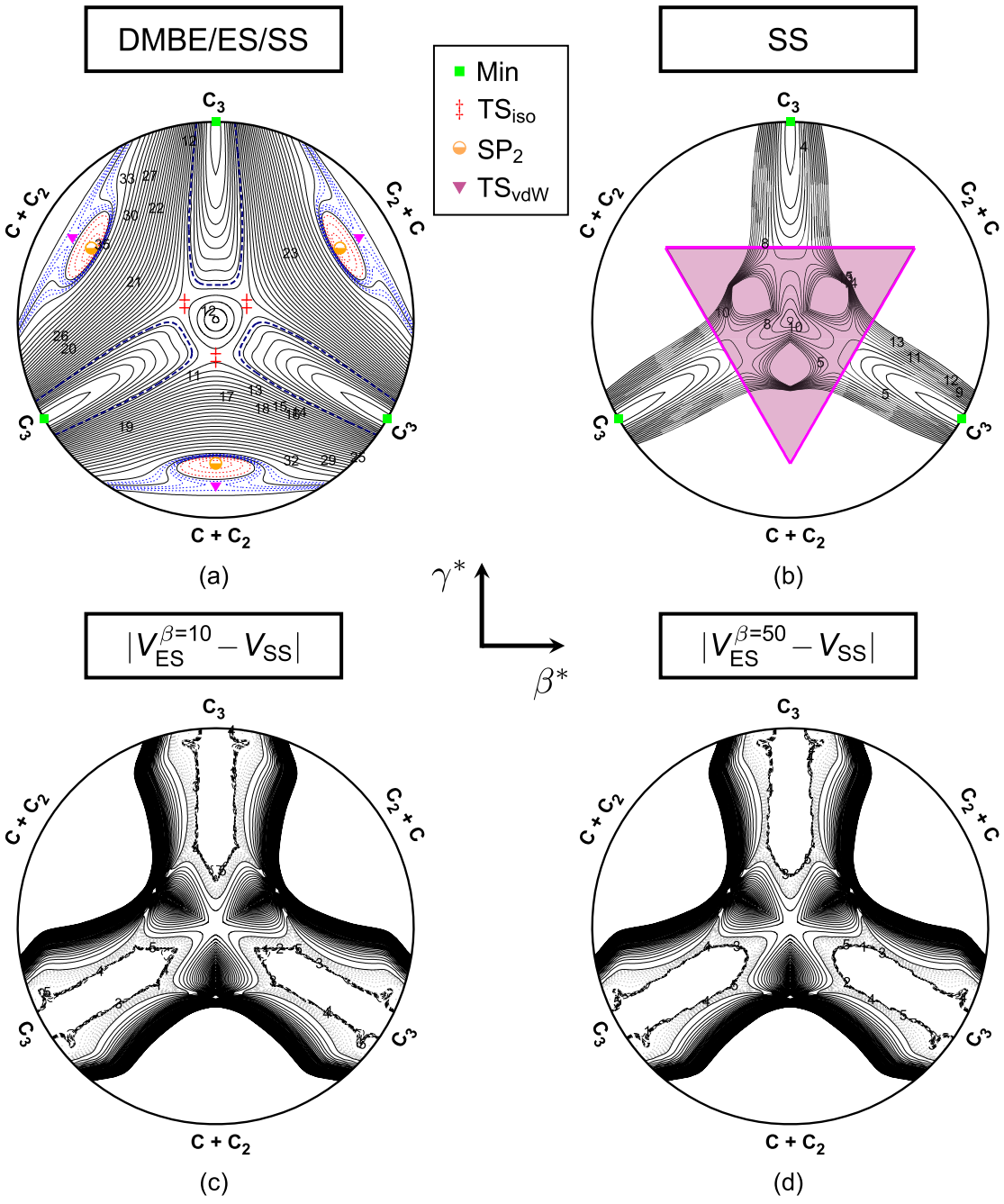

Fig. 1. Relaxed triangular plots in hyperspherical coordinates [40] of the ground-state C_3 PES. (a). DMBE/ES/SS potential (with $\beta = 50$). Black solid lines are equally spaced by 0.005 E_h, starting at −0.2904 E_h. Red and blue dashed lines are equally spaced by 0.001 E_h, starting at 0.00067 E_h and −0.0206 E_h, respectively. Navy dashed line defines the associated cutoff energy (E_0') in Eq. (4); see also Table 1. (b). SS potential. The PES has been shifted by −0.2904 E_h. Contours are equally spaced by 0.005 E_h, starting at −0.2904 E_h. Magenta triangle establishes the limits beyond which the corresponding local potential were delimited by a high repulsive wall in the rovibrational calculations. Panels (c) and (d) show contour plots of the absolute differences between the ES (with $\beta = 10$ and 50) and the corresponding SS potential. Black dashed, gray dotted and black solid lines are equally spaced by 10 cm^{-1}, 100 cm^{-1} and 1000 cm^{-1}, starting at 0 cm^{-1}, 50 cm^{-1} and 1000 cm^{-1}, respectively. See Refs. [28,31] for the stationary points. (For interpretation of the references to colour in this figure legend, the reader is referred to the web version of this article.)

Table 1
Parameters of the switching function $f'(\Delta E')$ [Eq. (4)] for the final ES PESs.

Parameter	DMBE/ES/SS
β	10/50
E_{min}/E_h	−0.2904
E_0'/E_h	−0.2619
n	2
ξ/E_h	1×10^{-12}

3. Rovibrational calculations

The rovibrational energy calculations have been carried out using the multidimensional discrete variable representation (DVR) method [41] as implemented in the DVR3D and ROTLEV3 suite of programs of Tennyson and co-workers [42]. All calculations employed orthogonal Jacobi coordinates with the molecular body-fixed z-axis embedded along r_1 (this is the CC diatomic distance, r_2 the C-CC center-of-mass separation, and θ the included angle; see Fig. S2 of the SM).

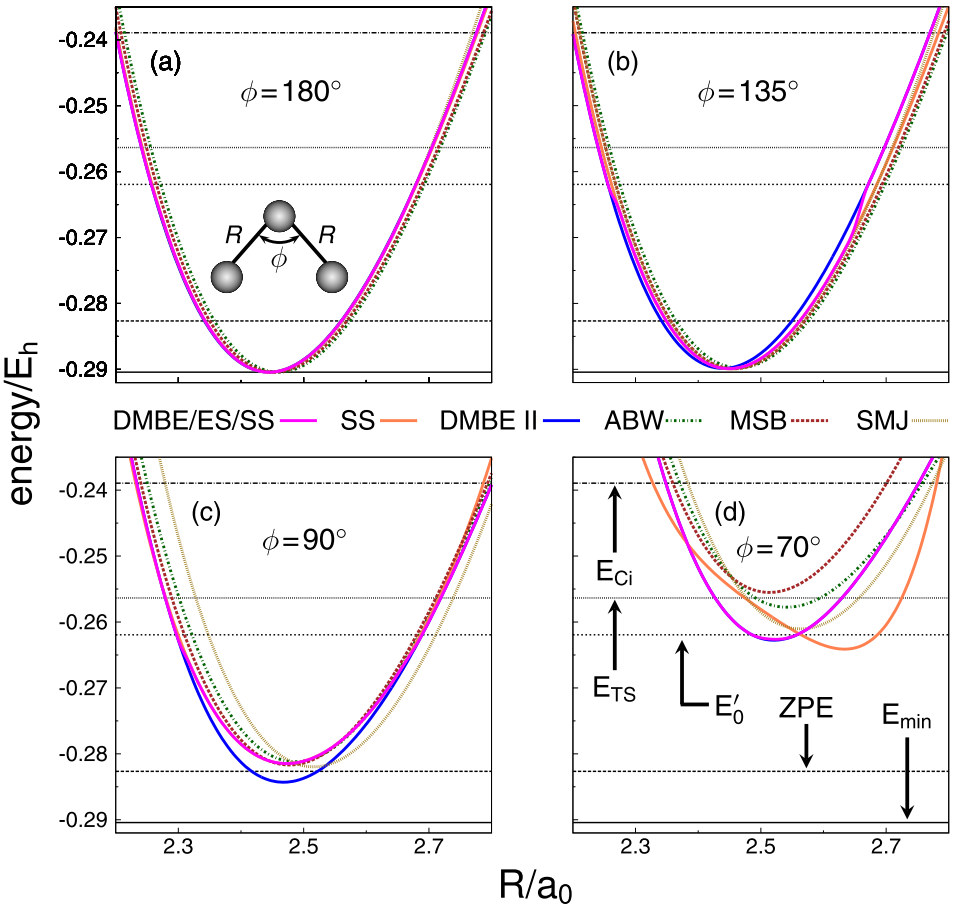

Fig. 2. Cuts of the DMBE/ES/SS (with $\beta = 50$), DMBE II, and corresponding local potentials along the symmetric stretching coordinate for fixed valence angles of $\phi = 180°, 135°, 90°$ and $70°$.

Table 2
Structural parameters (R_1, R_2 and ϕ), harmonic (w_i) and fundamental (ν_i) frequencies of the $C_3(^1\Sigma_g^+)$ global minima predicted from the ES and other potential forms.

Potential	R_1/a_0	R_2/a_0	ϕ/deg	w_1/cm^{-1}	w_2/cm^{-1}	w_3/cm^{-1}	ν_1[a]/cm^{-1}	ν_2[b]/cm^{-1}	ν_3[a]/cm^{-1}
DMBE/ES/SS[c]	2.445	2.445	180.0	1206.7	42.8	2101.3	1224.7	63.6	2039.9
SS[d]	2.445	2.445	180.0	1206.7	42.8	2101.3	1224.6	63.7	2039.6
DMBE II[e]	2.444	2.444	180.0	1203.9	61.0	2125.5	1234.1	60.8	2056.7
DMBE I[f]	2.444	2.444	180.0	1204.2	63.5	2126.5	1233.5	63.8	2061.3
ABW[g]	2.460	2.460	180.0	1214.5	65.0	2109.8	1219.1[h]	60.6[h]	2038.0[h]
							1226.8[i]	68.2[i]	2045.7[i]
MSB[j]	2.453	2.453	180.0	1201.3	41.5	2098.2	1218.9	64.7	2040.6
SMJ[k]	2.447	2.447	171.0	1195.6	32.2	2072.7	1224.0	62.9	2039.8
exp.	2.451	2.451[l]	180.0				1224.49[m]	63.86[m]	2040.02[m]
	2.445	2.445[n]	180.0						

[a] Calculated $(1, 0^0, 0)$ and $(0, 0^0, 1)$ vibrational band origins (for $J = \ell = 0$) relative to the ZPE level; see Section 4 for notation.
[b] Calculated $(0, 1^{1e}, 0)$ rovibrational band origin (for $J = \ell = 1$) relative to the ZPE level.
[c] This work.
[d] Ref. [35].
[e] Ref. [31].
[f] Ref. [28].
[g] Ref. [15].
[h] Ref. [15]. Relative to adjusted ZPE level at 1728.1 cm^{-1}.
[i] This work. Relative to calculated ZPE level at 1720.5 cm^{-1}.
[j] Ref. [34].
[k] Ref. [10].
[l] Ref. [36].
[m] Refs. [37,38].
[n] Mixed theoretical/experimental, Refs. [35,39].

In setting the so-called finite basis representation (FBR) [41], we have used Morse oscillator-like functions as radial vibrational basis whose parameters are summarized in Table S1 of the SM. For the angular basis, (associated) Legendre polynomials have been utilized [42]. With the above set of weighted orthogonal polynomials and their associated Gaussian quadratures (Table S1 shows the number of DVR pivots so employed), the FBR-to-DVR transformation ($\mathbf{H}^{DVR} = \mathbf{T}\mathbf{H}^{FBR}\mathbf{T}^{\dagger}$) has been accomplished by the so-called

Table 3
Lowest eigenvalues ($0,0^0,0$) for $J = \ell = 0$ as predicted from the ES and other forms.

	ZPE/cm^{-1}	
Potential[a]	Calculated[b]	Adjusted
DMBE/ES/SS[b]	1705.1	
SS[c]	1705.1	
DMBE II[d]	1714.5	
DMBE I[e]	1718.8	
ABW[f]	1720.5	1728.1[f]
MSB[g]	1702.0	
SMJ[h]	1687.9	

[a] The zero of energy is the corresponding C_3 global minimum in Table 2.
[b] This work.
[c] Ref. [35].
[d] Ref. [31].
[e] Ref. [28].
[f] Ref. [15].
[g] Ref. [34].
[h] Ref. [10].

quadrature approximation [41,42] with the corresponding kinetic energy integrals evaluated analytically prior to the transformation process. The final solutions are obtained from a series of diagonalizations and truncations of the transformed Hamiltonian ($\mathbf{H}^{\mathrm{DVR}}$) occurring in the order $r_2 \rightarrow r_1 \rightarrow \theta$.

The energy cutoff of $E_{\max}^{1D} = 70000\ \mathrm{cm}^{-1}$ (the global minima are the zero of the potentials) has been utilized for 1D problems and solutions with eigenenergies $\leqslant E_{\max}^{1D}$ were then used to construct 2D problems with maximum dimension of 1500. To built the final 3D matrix, such a dimension has been increased to 2500. All calculations were restricted to the levels reported in Ref. [15] for $J \leqslant 1$. They cover a range up to $\approx 8713\ \mathrm{cm}^{-1}$ above the corresponding ZPEs and are here typically converged to within $0.1\ \mathrm{cm}^{-1}$ or better. Excellent agreement (within $0.2\ \mathrm{cm}^{-1}$ or less) has been found between the calculated levels and those reported in the literature for all potential forms here utilized [10,15,34,35]. For $J = 1$, the two-step variational procedure of Tennyson and Sutcliffe [43] is employed. This uses the solutions of Coriolis decoupled "vibrational" problems (where the projection of J onto the body fixed z-axis, k, is assumed to be a good quantum number) as basis functions for the fully coupled rovibrational one [43], both for even(e) and odd(f)-parities. As stated in Section 2 and seen in Fig. 1(b) and S1, the SS and ABW forms show unphysical features near D_{3h} arrangements and hence the rovibrational calculations implied to use a cut-off with a high-energy wall near this region. The assumed borderlines are highlighted by the colored triangles. In contrast, the MSB [34] and SMJ [10] functions are well-behaved everywhere and could be utilized without prior modifications.

4. Results and discussion

Table S2 of the SM shows the differences between the observed [38,39,44–47] and calculated rovibrational levels for the DMBE/ES/SS PESs and SS local potential. Also given for comparison, are the values obtained from DMBE II [31], DMBE I [28], ABW [15], MSB [34] and SMJ [10] PESs. As for linear triatomic molecules, all energy levels are defined as (v_1, v_2^{ℓ}, v_3), where v_1 and v_3 are quantum numbers referring to symmetric and antisymmetric stretching, v_2 to bending, and $\ell = v_2, v_2 - 2, \ldots, 0$ or 1 is the vibrational angular momentum quantum number. Because degenerate levels ($\ell \neq 0$) occur only for $J \geq \ell$, all (v_1, v_2^1, v_3) band origins were calculated for $J = 1$ (see Section 3), with non-degenerate levels (v_1, v_2^0, v_3) obtained for $J = 0$. One should now comment on the assignment process. Although automated approaches have been successfully employed for triatomic molecules [12,16,18,48], the relatively modest number of states here considered (100 levels) allowed us to perform such assignments by visual inspection of the wave function plots (see Fig. S2). However, for excited overtones (typically, levels $> 6000\ \mathrm{cm}^{-1}$) such an approach can become cumbersome (even for automated assignments) as the wave functions show complex nodal structures. In fact, such intricate patterns of the eigenfunctions are specially manifested in the global PESs and can be attributed either to delocalization of the states or presence of "junctions" particularly at regions where the local and global forms mix together. Indeed, for the most complicated cases, assignments have been done in such a way as to minimize the discrepancies between the calculated and observed data. Table 4 and Fig. 3 gather the stratified rmsds for all 100 calculated levels up to

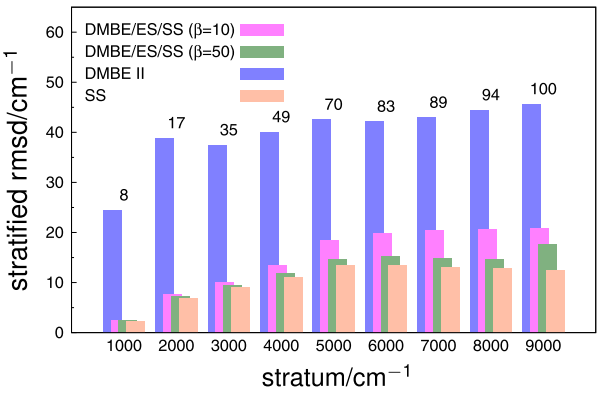

Fig. 3. Stratified rmsd for DMBE/ES/SS, DMBE II and SS PESs as a function of energy; see Table 4. The number of vibrational states up to indicated energy range is also given.

Table 4
Stratified rmsd (in cm^{-1}) for the 100 calculated rovibrational energy levels ($J = \ell \leq 1$) predicted from the ES and other forms.

		rmsd								
Energy[a]	N[b]	DMBE/ES/SS $\beta = 10$	DMBE/ES/SS $\beta = 50$	SS	DMBE II	DMBE I	ABW[c]	ABW[d]	MSB	SMJ
1000	8	2.5	2.4	2.3	24.5	32.5	3.2	7.1	9.5	1.2
2000	17	7.6	7.2	6.9	38.9	41.8	2.8	7.7	14.0	8.6
3000	35	10.0	9.5	9.1	37.5	47.0	2.6	8.4	13.5	34.4
4000	49	13.5	11.9	11.1	40.1	48.1	2.7	8.7	14.2	42.5
5000	70	18.5	14.7	13.5	42.6	49.4	2.7	8.1	16.2	38.2
6000	83	19.8	15.2	13.4	42.2	49.0	3.0	8.3	19.3	41.1
7000	89	20.4	14.8	13.0	43.0	50.4	3.0	8.2	22.3	43.8
8000	94	20.7	14.6	12.9	44.5	52.1	2.9	8.2	25.4	47.9
9000	100	20.9	17.7	12.5	45.7	53.4	2.9	8.2	28.6	55.9

[a] Units of energy are cm^{-1}. Energy strata relative to the corresponding ZPE level; see Table 3.
[b] Number of vibrational states up to indicated energy range.
[c] Energy relative to the adjusted ZPE level at 1728.1 cm^{-1}.
[d] Energy relative to the (true) calculated ZPE level at 1720.5 cm^{-1}.

$\approx 8713\ cm^{-1}$ above ZPE. As shown, the calculated energies from the ES potentials agree well with those obtained using the corresponding SS form. Obviously, this is particularly so for the case of $\beta = 50$. Globally, the DMBE/ES/SS PESs show rmsds with respect to experimental term values of 20.9 and 17.7 cm^{-1} for $\beta = 10$ and 50, respectively. These are to be compared with the corresponding rmsd of 12.5 cm^{-1} obtained from the SS PES. Indeed, as Fig. 1(c) and (d) show, the absolute differences between the ES and local forms are minimal at the physically acceptable region covered by this latter. Expectedly [7], small discrepancies appear with increasing energy as apparent from the final stratified rmsd (see Fig. 4).

Since the DMBE II and SS components differ only slightly near the global minimum, no marked scars arise at their merging together; see Fig. 2(a). They are more apparent though at some geometries far away from this region; Fig. 2(b). As shown in Fig. 2(a), the DMBE II [31], SS [35], and SMJ [10] potentials are nearly indistinguishable at linear geometries; Table 2. Recall that the empirical SMJ surface [10] has its equilibrium configuration at non-linear arrangements ($R_1 = R_2 = 2.447\ a_0$ and $\phi = 171.6°$) despite mimicking (rmsd = 8.6 cm^{-1}) term values up to 2000 cm^{-1}. Note further that the ABW form [15] reproduces all levels with a rmsd of 8.2 cm^{-1} when the ZPE is the calculated value, but its equilibrium geometry is somewhat at variance with all others; Fig. 2(a).

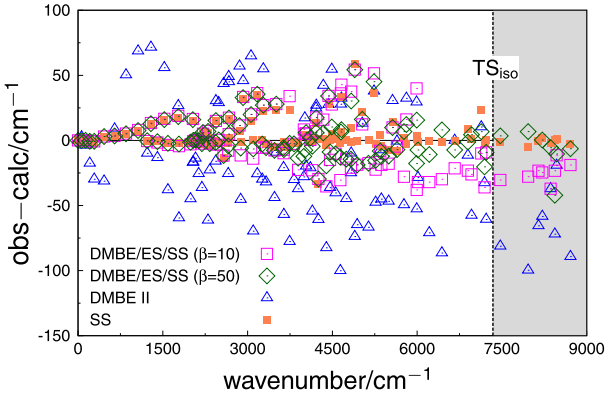

Fig. 4. Scatter plot of errors (observed-calculated) for DMBE/ES/ SS, DMBE II and SS PESs as a function of the band centers. The vertical line indicates the isomerization transition state TS_{iso} energy.

Of course, one would like to enhance the accuracy of the global DMBE/ES/SS potential by bringing it into agreement with the SS surface at regions where the latter is physically meaningful. This may be achieved by varying the values of (i) E_0' and/or (ii) β in Eq. (4). The first cannot be considered due to spurious features arising in the local form. As for (ii), a few attempts have been done to bring the DMBE/ES/SS spectroscopy into an even closer agreement with SS at the higher energy strata by increasing β. This would tend to enhance the visibility of the region where the two forms merge into one another, which might originate some instability in dynamics studies (undetected thus far). Yet, a reduction of 30 cm^{-1} in the final rmsd for levels up to 9000 cm^{-1} is already a significant asset of the ES approach. Of course, its major virtue is to graft the proper asymptotic behavior into a near-spectroscopic local PES. Naturally, the accuracy of the ES method hinges on the quality of its components: if better forms become available (either the global or local parts), their mere replacememt will yield an improved ES form.

Despite significant improvements of the SS PES with respect to the MSB form [34] in reproducing spectroscopic constants and term energies for the low-lying states, some deficiencies remain, particularly in describing excited bending overtones [the deviation here obtained for the $(0,18^0,0)$ state at 1773.37 cm^{-1} is as high as 17.6 cm^{-1}]. Note that the MSB form has been calibrated from

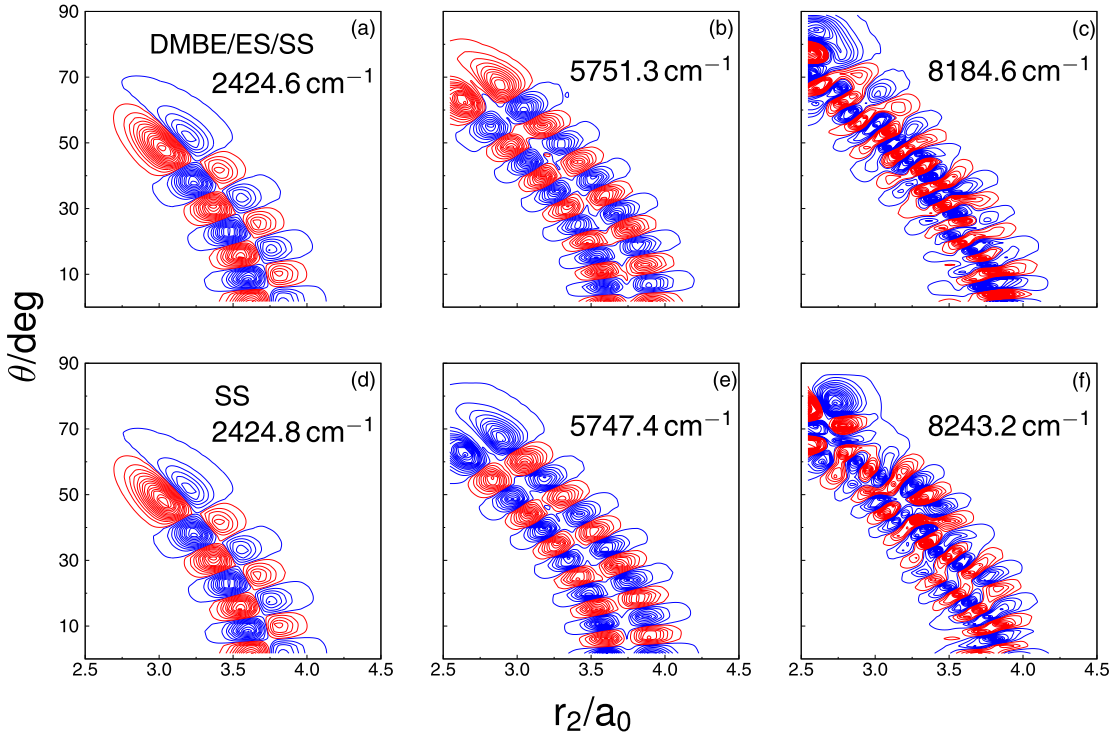

Fig. 5. Contour plots of sample vibrational wave functions for $J = \ell = 0$ calculated on DMBE/ES/SS [panels (a)–(c)] and SS [panels (d)–(f)] PESs at distinct energy regimes. Panels (a) and (d) depict $(1,12^0,0)$ wave functions, while (b) and (e) are for $(1,24^0,1)$. For comparison, panels (c) and (f) show sample wave functions with similar nodal structures in the energy range of 8000–8500 cm^{-1} above ZPE. Blue and red lines are for negative and positive contours, respectively.

CCSD(T) calculations with a basis set of near (T/Q)Z quality [in a total of 108 points], and hence is likely less reliable in reproducing experimental band centers and rotational manifolds. This is apparent from Table 4, where a rmsd as high as 28.6 cm^{-1} is visible. However, we should note that Mladenović et al. [34] only attempted a reliable representation up to 3000 cm^{-1} above equilibrium. Despite being primarily concerned with low-lying rotation-vibration energies only ($\approx$ 3500 cm^{-1} above the ZPE), Schröder and Sebald [35] calibrated their surface from geometries with valence angles up to 80° ($\approx$ 6000 cm^{-1} above equilibrium) which justifies its use for the purpose here envisaged.

As already noted, none of the near-equilibrium forms describe the saddle point TS_{iso} which is responsible for the isomerization involving the three symmetry related $C_3(^1\Sigma_g^+)$ global minima [28,31]. Although such potentials adequately account for the large amplitude vibrational motion in C_3 at low-to-intermediate energies, one must expect inadequacies due to delocalization of highly excited rovibrational eigenstates lying close to or above the isomerization barrier. As noted elsewhere [49,50] such effects are particularly relevant in studying unimolecular reactions and intramolecular vibrational redistribution processes in floppy systems.

Fig. 5 shows sample vibrational wave functions obtained from the DMBE/ES/SS potential and the corresponding local form at distinct energy regimes. Note that no attempt has been made to assign wave functions with complicated nodal structures such as the ones in panels (c) and (f). Overall, for low-to-intermediate excitation energies, the vibrational wave functions so obtained from both ES and local potentials exhibit quite close behavior; cf. panels (a)/(d) and (b)/(e). The very delocalized nature of the vibrational wave function can be best seen in the plots shown in panels (c) and (f). In contrast to its SS counterpart, such eigenfunction can actually surpass (or tunnel through) the potential barrier and delocalize over any of the three symmetry related minima. Indeed, the task of calculating accurate energies and wave functions for such high-lying states can be a difficult one, particularly when covering regions of the nuclear configuration space at which crossings between surfaces are known to exist [32]. At such regions, nonadiabatic effects are ubiquitous and therefore, the accuracy of adiabatic calculations is limited. In fact, for ground-state $C_3(1^1A')$, it is fair to think that many of the rovibrational states lying halfway between ZPE and the conical intersections (5000 cm^{-1} above ZPE) are perturbed by interactions with the first excited $2^1A'$ state [28,31,32]. For this reason, we judge the present methodology to be reliable for levels under 4500 cm^{-1} or so above ZPE. Of course, one might struggle for a more accurate spectroscopic PES by employing an hybrid approach [14] through which the Taylor-series-type expansions are refined (by fitting experimental rovibrational data) once embedded in the global DMBE PES. Yet, we must recall the impossibility of properly assigning highly excited vibrational states (see above) and bear in mind that such a PES would lie beyond the strict Born-Oppenheimer sense. Needless to say, all forms here studied lack the possibility of including nonadiabatic effects (but the geometrical phase when describing the crossing seams) due to their single-sheeted nature.

5. Conclusions

We have reported an energy-switching form for ground-state C_3 that mimics with near spectroscopic accuracy the rovibrational spectrum of the title triatomic cluster in regions where nonadiabatic effects are expected to be small, while describing all other key topological attributes as best known thus far. Further progress can be done if so justified by combining the approach with a least squares fit of the rovibrational energies as described in past work [12,16,18]. To summarize, the approach utilized in the present work involves minimal cost, avoids complicated issues associated with the assignment of levels close to isomerization, and produced a global form that can be commended for most dynamical studies ahead.

Acknowledgments

This work is supported by Fundação para a Ciência e a Tecnologia and Coimbra Chemistry Centre, Portugal, through the project UI0313/QUI/2013, also co-funded by FEDER/COMPETE 2020-EU. C.M. thanks also the CAPES Foundation (Ministry of Education of Brazil) for a scholarship (Process BEX 0417/13-0).

Appendix A. Supplementary material

Supplementary data associated with this article can be found, in the online version, at https://doi.org/10.1016/j.cplett.2018.04.005.

References

[1] P.J. Kuntz, Features of Potential Energy Surfaces and Their Effect on Collisions, Springer US, 1976, pp. 53–120, Ch. 2 <http://www.springer.com/us/book/9781475706468> .
[2] J.S. Wright, S.K. Gray, Rotated morse curve-spline potential function for A+BC reaction dynamics: application to (Cl, HBr), (F,H_2), and (H^+,H_2), J. Chem. Phys. 69 (1978) 67–81, https://doi.org/10.1063/1.436347.
[3] J.N.L. Connor, Reactive molecular collision calculations, Comp. Phys. Comm. 17 (1979) 117–143, https://doi.org/10.1016/0010-4655(79)90075-4.
[4] A.J.C. Varandas, Intermolecular and intramolecular potentials: topographical aspects, calculation, and functional representation via a double many-body expansion method, Adv. Chem. Phys. 74 (1988) 255–338, https://doi.org/10.1002/9780470141236.ch2.
[5] R. Marquardt, M. Quack, Global Analytical Potential Energy Surfaces for High-resolution Molecular Spectroscopy and Reaction Dynamics, John Wiley & Sons, 2011, pp. 511–549, https://doi.org/10.1002/9780470749593.hrs013, Ch. 12.
[6] A.J.C. Varandas, Energy switching approach to potential surfaces: an accurate single–valued function for the water molecule, J. Chem. Phys. 105 (1996) 3524–3531, https://doi.org/10.1063/1.473005.
[7] A.J.C. Varandas, Energy switching approach to potential surfaces. II. Two-valued function for the water molecule, J. Chem. Phys. 107 (1997) 867–878, https://doi.org/10.1063/1.474385.
[8] R. Prosmiti, O.L. Polyansky, J. Tennyson, A global potential energy surface for the H_3^+ molecule, Chem. Phys. Lett. 273 (1997) 107–114, https://doi.org/10.1016/S0009-2614(97)00596-4.
[9] A.J.C. Varandas, A.I. Voronin, P.J.S.B. Caridade, Energy switching approach to potential surfaces. III. Three-valued function for the water molecule, J. Chem. Phys. 108 (1998) 7623–7630, https://doi.org/10.1063/1.476197.
[10] V. Špirko, M. Mengel, P. Jensen, Calculation of rotation-vibration energy levels in ground state C_3 by a born-oppenheimer-type separation of the vibrational motions, J. Mol. Spectrosc. 183 (1997) 129–138, https://doi.org/10.1006/jmsp.1996.7257.
[11] O.L. Polyansky, R. Prosmiti, W. Klopper, J. Tennyson, An accurate, global, *Ab Initio* potential energy surface for the H_3^+ molecule, Mol. Phys. 98 (2000) 261–273, https://doi.org/10.1080/00268970009483290.
[12] A.J.C. Varandas, S.P.J. Rodrigues, A realistic double many-body expansion potential energy surface for $SO_2(\widetilde{X}^1A')$ from a multiproperty fit to accurate *ab initio* energies and vibrational levels, Spectrochim. Acta Mol. Biomol. Spectrosc. 58 (2002) 629–647, https://doi.org/10.1016/S1386-1425(01)00661-8.
[13] S. Yurchenko, M. Carvajal, P. Jensen, F. Herregodts, T. Huet, Potential parameters of PH_3 obtained by simultaneous fitting of *ab initio* data and experimental vibrational band origins, Chem. Phys. 290 (2003) 59–67, https://doi.org/10.1016/S0301-0104(03)00098-3.
[14] A.J.C. Varandas, A realistic multi-sheeted potential energy surface for $NO_2(^2A')$ from the double many-body expansion method and a novel multiple energy-switching scheme, J. Chem. Phys. 119 (2003) 2596–2613, https://doi.org/10.1063/1.1586911.
[15] K. Ahmed, G.G. Balint-Kurti, C.M. Western, *Ab initio* calculations and vibrational energy level fits for the lower singlet potential-energy surfaces of C_3, J. Chem. Phys. 121 (2004) 10041–10051, https://doi.org/10.1063/1.1806820.
[16] A.J.C. Varandas, S.P.J. Rodrigues, New double many-body expansion potential energy surface for ground-state HCN from a multiproperty fit to accurate *ab initio* energies and rovibrational calculations, J. Phys. Chem. A 110 (2006) 485–493, https://doi.org/10.1021/jp051434p.
[17] B.R.L. Galvão, S.P.J. Rodrigues, A.J.C. Varandas, Energy-switching potential energy surface for the water molecule revisited: a highly accurate singled-

sheeted form, J. Chem. Phys. 129 (2008) 044302–044308, https://doi.org/10.1063/1.2953580.
[18] S. Rodrigues, A. Fontes, Y. Li, A. Varandas, Refining to near spectroscopic accuracy the double many-body expansion potential energy surface for ground-state NH_2, Chem. Phys. Lett. 516 (2011) 17–22, https://doi.org/10.1016/j.cplett.2011.09.050.
[19] X. Huang, D.W. Schwenke, S.A. Tashkun, T.J. Lee, An isotopic-independent highly accurate potential energy surface for CO_2 isotopologues and an initial $^{12}C^{16}O_2$ infrared line list, J. Chem. Phys. 136 (2012) 124311–124327, https://doi.org/10.1063/1.3697540.
[20] I.I. Mizus, A.A. Kyuberis, N.F. Zobov, V.Y. Makhnev, O.L. Polyansky, J. Tennyson, High-accuracy water potential energy surface for the calculation of infrared spectra, Phil. Trans. R. Soc. A 376 (2018) 1–11, https://doi.org/10.1098/rsta.2017.0149.
[21] O.L. Polyansky, N.F. Zobov, I.I. Mizus, A.A. Kyuberis, L. Lodi, J. Tennyson, Potential energy surface, dipole moment surface and the intensity calculations for the 10 μm,5 μm and 3 μm bands of ozone, J. Quant. Spectrosc. Radiat. Transfer 210 (2018) 127–135, https://doi.org/10.1016/j.jqsrt.2018.02.018.
[22] A.J.C. Varandas, A general approach to the potential energy functions of small polyatomic systems: molecules and van der Waals Molecules, J. Mol. Struct.: THEOCHEM 120 (1985) 401–424, https://doi.org/10.1016/0166-1280(85)85134-4.
[23] A.J.C. Varandas, S.P.J. Rodrigues, P.A.J. Gomes, Energy switching potential energy surfaces and spectra of the Van der Waals modes for the ArHCN molecule, Chem. Phys. Lett. 297 (1998) 458–466, https://doi.org/10.1016/S0009-2614(98)01159-2.
[24] H.G. Yu, A.J.C. Varandas, *Ab initio* theoretical calculation and potential energy surface for ground-state HO_3, Chem. Phys. Lett. 334 (2001) 173–178, https://doi.org/10.1016/S0009-2614(00)01432-9.
[25] W.H. Ansari, A.J.C. Varandas, Six-dimensional energy-switching potential energy surface for HeHCN, J. Phys. Chem. A 106 (2002) 9338–9344, https://doi.org/10.1021/jp021209x.
[26] A. Van Orden, R.J. Saykally, Small carbon clusters: spectroscopy, structure, and energetics, Chem. Rev. 98 (1998) 2313–2358, https://doi.org/10.1021/cr970086n.
[27] A.J.C. Varandas, C.M.R. Rocha, C_n(n=2-4): current status, Phil. Trans. R. Soc. A 376 (2018) 1–46, https://doi.org/10.1098/rsta.2017.0145.
[28] C.M.R. Rocha, A.J.C. Varandas, Accurate *ab initio*-based double many-dody expansion potential energy surface for the adiabatic ground-state of the C_3 radical including combined Jahn-Teller plus Pseudo-Jahn-Teller interactions, J. Chem. Phys. 143 (2015) 074302–074318, https://doi.org/10.1063/1.4928434.
[29] T.H. Dunning, A road map for the calculation of molecular binding energies, J. Phys. Chem. A 104 (2000) 9062–9080, https://doi.org/10.1021/jp001507z.
[30] A.J.C. Varandas, A semiempirical method for correcting configuration interaction potential energy surfaces, J. Chem. Phys. 90 (1989) 4379–4391, https://doi.org/10.1063/1.456624.
[31] C.M.R. Rocha, A.J.C. Varandas, Multiple conical intersections in small linear parameter Jahn-Teller systems: the DMBE potential energy surface for ground-state C_3 revisited, Phys. Chem. Chem. Phys. doi:https://doi.org/10.1039/C7CP06656B.
[32] C.M.R. Rocha, A.J.C. Varandas, The Jahn-Teller plus Pseudo-Jahn-Teller vibronic problem in the C_3 radical and its topological implications, J. Chem. Phys. 144 (2016) 064309–064324, https://doi.org/10.1063/1.4941382.
[33] P. Jensen, C.M. Rohlfing, J. Almlöf, Calculation of the complete-active-space self-consistent-field potential-energy surface, the dipole moment surfaces, the rotation-vibration energies, and the vibrational transition moments for $C_3(\tilde{X}^1\Sigma_g^+)$, J. Chem. Phys. 97 (1992) 3399–3411, https://doi.org/10.1063/1.462976.
[34] M. Mladenović, S. Schmatz, P. Botschwina, Large-scale *ab initio* calculations for C_3, J. Chem. Phys. 101 (1994) 5891–5899, https://doi.org/10.1063/1.467305.
[35] B. Schröder, P. Sebald, High-level theoretical rovibrational spectroscopy beyond fc-CCSD(T): the C_3 molecule, J. Chem. Phys. 144 (2016) 044307–044318, https://doi.org/10.1063/1.4940780.
[36] K.W. Hinkle, J.J. Keady, P.F. Bernath, Detection of C_3 in the circumstellar shell of IRC+10216, Science 241 (1988) 1319–1322, https://doi.org/10.1126/science.241.4871.1319.
[37] G. Zhang, K. Chen, A.J. Merer, Y. Hsu, W. Chen, S. Shaji, Y. Liao, The 4051-Å band of C_3 ($\tilde{A}^1\Pi_u - \tilde{X}^1\Sigma_g^+$,000-000): perturbed low-J lines and lifetime measurements, J. Chem. Phys. 122 (2005) 244308–244315, https://doi.org/10.1063/1.1928827.
[38] J. Krieg, V. Lutter, C.P. Endres, I.H. Keppeler, P. Jensen, M.E. Harding, J. Vázquez, S. Schlemmer, T.F. Giesen, S. Thorwirth, High-resolution spectroscopy of C_3 around 3 μm, J. Phys. Chem. A 117 (2013) 3332–3339, https://doi.org/10.1021/jp3119204.
[39] A.A. Breier, T. Büchling, R. Schnierer, V. Lutter, G.W. Fuchs, K.M.T. Yamada, B. Mookerjea, J. Stutzki, T.F. Giesen, Lowest bending mode of ^{13}C-substituted C_3 and an experimentally derived structure, J. Chem. Phys. 145 (2016) 234302–234311, https://doi.org/10.1063/1.4971854.
[40] A.J.C. Varandas, A useful triangular plot of triatomic potential energy surfaces, Chem. Phys. Lett. 138 (1987) 455–461, https://doi.org/10.1016/0009-2614(87)80540-7.
[41] J.C. Light, T. Carrington, Discrete-Variable Representations and their Utilization, John Wiley & Sons Inc., 2007, pp. 263–310, https://doi.org/10.1002/9780470141731.ch4, Ch. 4.
[42] J. Tennyson, M.A. Kostin, P. Barletta, G.J. Harris, O.L. Polyansky, J. Ramanlal, N.F. Zobov, DVR3D: A program suite for the calculation of rotation-vibration spectra of triatomic molecules, Comput. Phys. Commun. 163 (2004) 85–116, https://doi.org/10.1016/j.cpc.2003.10.003.
[43] J. Tennyson, B.T. Sutcliffe, Highly rotationally excited states of floppy molecules: H_2D^+ with J≤20, Mol. Phys. 58 (1986) 1067–1085, https://doi.org/10.1080/00268978600101811.
[44] E.A. Rohlfing, Laser-induced-fluorescence spectroscopy of jet-cooled C_3, J. Chem. Phys. 91 (1989) 4531–4542, https://doi.org/10.1063/1.456791.
[45] C.A. Schmuttenmaer, R.C. Cohen, N. Pugliano, J.R. Heath, A.L. Cooksy, K.L. Busarow, R.J. Saykally, Tunable Far-IR laser spectroscopy of jet-cooled carbon clusters: the ν_2 bending vibration of C_3, Science 249 (1990) 897–900, https://doi.org/10.1126/science.11538082.
[46] E.A. Rohlfing, J.E.M. Goldsmith, Stimulated-emission pumping spectroscopy of jet-cooled C_3: antisymmetric stretch-bend levels, J. Opt. Soc. Am. B 7 (1990) 1915–1923, https://doi.org/10.1364/JOSAB.7.001915.
[47] F.J. Northrup, T.J. Sears, Stimulated-emission pumping spectroscopy study of jet-cooled C_3: pure bending levels and bend-symmetric-stretch combination levels of $X^1\Sigma_g^+$, J. Opt. Soc. Am. B 7 (1990) 1924–1934, https://doi.org/10.1364/JOSAB.7.001924.
[48] M. Menou, C. Leforestier, Labeling the HCN vibrational states in the regular spectrum, Chem. Phys. Lett. 210 (1993) 294–302, https://doi.org/10.1016/0009-2614(93)89136-6.
[49] Z. Bačić, J.C. Light, Theoretical methods for rovibrational states of floppy molecules, Annu. Rev. Phys. Chem. 40 (1989) 469–498, https://doi.org/10.1146/annurev.pc.40.100189.002345.
[50] Z. Bačić, Accurate calculation and assignment of highly excited vibrational levels of floppy triatomic molecules in a basis of adiabatic vibrational eigenstates, J. Chem. Phys. 95 (1991) 3456–3466, https://doi.org/10.1063/1.461798.